Composition Dependent Miscibility in the Crystalline State of Polyamide

6 /Polyamide 4,10 Blends: from Single to Double Crystalline Blends

Maryam Safari [1], Itziar Otaegi [1], Nora Aramburu [1], Yu Wang [2,3], Guoming Liu [2,4]*, Xia

Dong [2,4], Dujin Wang [2,4], Gonzalo Guerrica-Echevarria [1], Alejandro J. Müller [1,5]*

[1] *POLYMAT and Department of Polymers and Advanced Materials: Physics, Chemistry

and Technology, Faculty of Chemistry, University of the Basque Country UPV/EHU,

Paseo Manuel de Lardizabal, 3, 20018 Donostia-San Sebastián, Spain*

[2] *CAS Key Laboratory of Engineering Plastics, CAS Research/Education Center for

Excellence in Molecular Sciences, Beijing National Laboratory for Molecular Sciences,

Institute of Chemistry, Chinese Academy of Sciences, Beijing 100190, China*
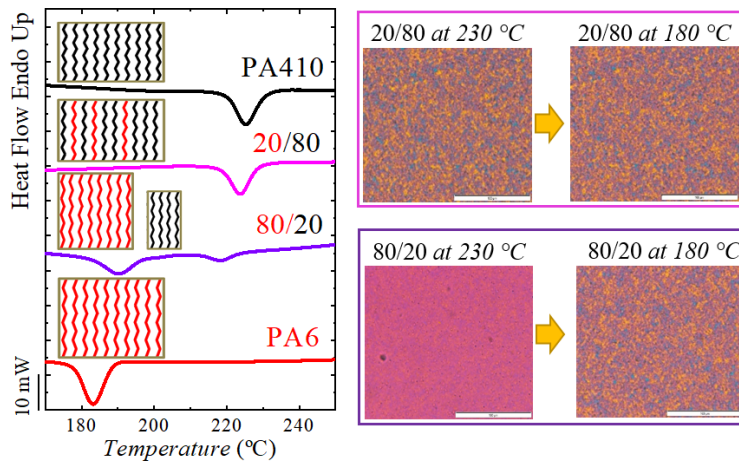
[3] *Shenzhen Key Laboratory of Polymer Science and Technology, College of Materials

Science and Engineering, Shenzhen University, Shenzhen 518060, China*

[4] *University of Chinese Academy of Sciences, Beijing 100049, China*

[5] *IKERBASQUE, Basque Foundation for Science, Bilbao, 48009, Spain*

*Corresponding authors: gmliu@iccas.ac.cn, alejandrojesus.muller@ehu.es.

Abstract

We study the composition-dependent miscibility of polyamide 6 and biobased polyamide 4,10 (PA6/PA410) blends, as triggered by crystallization driven phase segregation. The blends were prepared by extrusion in a wide composition range and studied by X-ray diffraction (both *in-situ* and *ex-situ* SAXS/WAXS), Differential Scanning Calorimetry (DSC), and Polarized Light Optical Microscopy (PLOM) during non-isothermal crystallization. The blends were miscible in the amorphous state, as demonstrated by a single T_g that follows the Fox equation as a function of composition. The blends were also considered to be miscible in the melt, as no evidence of phase segregation was found by SAXS or phase contrast microscopy in the melt. Remarkably, the blends can also be miscible in the crystalline state in a limited composition range. When only 10 or 20% PA6 is present in the blends, co-crystallization was evidenced by DSC and WAXS and the blends exhibited a single PA410 rich crystalline phase. On the other hand, as 30% or more PA6 is added to PA410, crystallization driven phase segregation occurs and progressively increased with PA6 content in the blends. Hence double crystalline blends are formed with both PA6 rich and PA410 rich crystalline phases. Clear evidence of the presence of either one or two crystalline phases was obtained by temperature-dependent measurements employing DSC, PLOM, WAXS and SAXS. Both the single and double crystalline PA6/PA410 blends exhibited good mechanical properties in view of the excellent compatibility displayed by the blends. The mechanical properties are in line with those exhibited by miscible blends following a simple rule of mixtures.

Key words: biopolymers; polyamide blends; mechanical properties; nylon 6; nylon 4,10.

INTRODUCTION

Concern about the use of petrochemical polymers in the plastics industry has grown more intense over the last decade, and efforts made towards their replacement with polymers extracted from renewable resources are gaining strength. Biobased polymers production is predicted to increase from around 5 million tons in 2013 to about 17 million tons in 2020 [1]. This is a result of a combination of factors including a growing concern for sustainable development together with a higher demand for sustainable products and the improved price-performance characteristics of newly developed bioplastics resulting from recent technological improvements.

Polyamides (PAs) or nylons have traditionally been used as fibres for the manufacture of fabrics, but nowadays they are used in many applications, from carpets [2] to injection moulded and extruded engineering parts [3]. For example, polyamide 4,10 (PA410) is used in the automotive industry for the fabrication of engine and crankshaft covers. Polyamides are extensively used engineering thermoplastics, which represent a success in the polymer composites industry due to their excellent thermo-mechanical properties, and nowadays many different polyamide grades are commercially available, including various filler-reinforced materials. The replacement of traditional petrochemical polyamides with others obtained from renewable resources would result in the development of a range of environmentally more sustainable materials, which seems to be the trend in the near future [4-7]. In this sense, PA blends of traditional and frequently used PAs, such as PA6 or PA66, with newly commercially available bio-PAs, either totally or partially derived from renewable resources, arise as a halfway solution and, therefore, the study of these blends is imperative.

4

Melt blending is the preferred method in the industry for the fabrication of polymeric products, because it is solvent-free, cost-effective, fast, and does not need specific types of equipment [8]. Literature concerning polyamide blends focuses largely on PA6 blended with PP [9-11], ABS [12-14], PE [15-17], PA66 [18], PET [19] , long chain polyamides (LCPAs) [20] and different rubbers [21-22], the majority of which are immiscible systems. Polyamide-polyamide blend literature consists primarily of studies on aliphatic/aromatic polyamide blends [23-29], whereas little work has been performed on aliphatic/aliphatic blends [2, 6-7, 30-32]. In addition, few works have been reported on biobased polymer blends for durable high performance applications [33-37], while studies concerning biodegradable polymer blends for either biomedical or packaging applications are numerous [33, 38-46].

Miscibility is an important factor that must be considered in polymeric blends. A single glass transition temperature (T_g) and a melting point (T_m) reduction are the most important evidences for miscibility. Macromolecules are characterized by long chains that limit mixing entropy to rather small values, therefore miscible polymer blends are infrequent. The enthalpy of mixing can be large enough in some cases to induce positive free energy of mixing, indicating that polymer mixing is not a thermodynamically spontaneous process. Consequently, the majority of polymers exhibit phase-separation when mixed. Most of the self-associated polyamide blends are immiscible [6,7]. However, transamidation reaction can occur at high temperatures [20], and improve miscibility, due to the formation of a copolymer at the interphase. For very small or negative enthalpies of mixing, the polymer mixture is miscible. It is well known that the typically coarse morphology of immiscible blends usually results in undesirable physical properties. Indeed, research on polymer blending has been devoted, to a large extent, to study the results of the

5

addition of different compatibilization agents and the use of novel blending procedures on their morphology and properties [9, 12-14, 33, 35, 47-54]. Obviously, if compatibilization is not required, blending becomes quicker and cheaper. Thus, miscible polymer blends are highly interesting from an industrial point of view. Miscible aliphatic polyamide blends are scarce and include (PA48/PA66) [30], (PA66/PA6) [32, 55], (PA410/PA610) [3] and (PA11/PA610) [2]. For these miscible blends, the quantity of methylene units linking the amide groups along the chain is very similar.

In a previous study [56], PA410 was melt mixed with up to 25% of PA6, and some evidences of miscibility between both polyamides were observed in this limited composition range. The blends displayed a single glass transition temperature, which could be fitted to the Fox equation, thus indicating full miscibility in the amorphous phase over the composition range under study. On the other hand, DSC results pointed to possible mixed crystalline phases and co-crystallization of both polyamides in the blends, at least in the mentioned limited range. However, the studied composition range was very limited and no X-ray scaterring measurements were performed to support possible co-crystallization. So far, very few semicrystalline polymers are known to be miscible with one another (forming double crystalline polymer blends), and the resulting blends exhibit remarkable kinetic and structural properties [57].

The objective of this work is to study the miscibility, structure and physical properties of novel aliphatic semicrystalline polyamide blends, namely PA410, which is derived from renewable castor oil, and PA6, whose origin is petrochemical, over the whole range of compositions. Several characterization techniques were applied including Polarized Light Optical Microscopy (PLOM), Differential Scanning Calorimetry (DSC),

6

and both Wide and Small Angle X-ray Scattering (WAXS/SAXS). We have obtained remarkable matching DSC and X-ray evidence that demonstrate that for the blends are miscible in the melt and amorphous state and can even co-crystallize in a limited composition range (i.e., they are also miscible in the crystalline state).

EXPERIMENTAL SECTION

Materials

Two types of polyamides (PAs), namely PA410 , supplied by DSM (EcoPaXX® Q150-D, Genk, Belgium) and PA6, provided by Lanxess (Durethan® B30S, Cologne, Germany), were used. PA410 was melt blended with PA6 at PA6/PA410 wt % ratio of 0/100, 10/90, 20/80, 30/70, 40/60, 50/50, 60/40, 70/30, 80/20, 90/10 and 100/0. To avoid moisture-induced degradation reactions, both PA410 and PA6 were completely dried using a Wittmann Drymax air dryer (Kottingbrunn, Austria) around 60 h at a temperatute of 80 °C. The PA6/PA410 blends were prepared by melt-mixing method using a co-rotating twin screw extruder-kneader (Collin ZK 25T SCD 15 Teach-Line, Ebersberg, Bavaria, Germany) with screw rotation speed of 200 rpm and at 260 °C. The diameter and L/D ratio of the extruder screws were 25 and 18 mm.

A water bath was used to cool down the extrudates, then the samples were pelletized and fully dried again. Injection moulding process was performed by using a reciprocating screw injection moulding machine (Battenfeld PLUS 350/75, Kottingbrunn, Austria). A 25 mm diameter screw and a 14 L/D ratio were employed. The injection molding press closing force was 350 kN. Samples for tensile (sample thickness = 2 mm,

ASTM D-638, type IV) and impact (sample thickness = 3.2 mm, ASTM D-256) testing were obtained. The melt and mould temperatures were set at 260 °C and 85 °C, respectively. The pressure time, injection rate, and cooling time were set to 3 s, 42 cm^3/s and 15 s, correspondingly. To avoid the humidity absorption after the blend preparation, all samples were stored in a desiccator.

Methods

Differential Scanning Calorimetry (DSC). A Perkin-Elmer DSC 8500 calorimeter was employed. Tests were made under an ultra pure nitrogen atmosphere with a flow rate of 20 ml/min and using tin and indium as calibration standards. All samples were vacuum dried at 80 ºC overnight. Approximately 5 mg were placed inside DSC aluminium pans and well sealed. DSC heating scans were performed first from room temperature to 280 °C (that is 30 °C above their melting points) and held at this temperature for 3 min in order to erase any preserved thermal history. Then, they were cooled down to 100 °C and heated up again to 280 ºC. All measurements were done at 20 °C/min and the melting temperature T_m was determined as the temperature of the main peak in the second DSC scan.

Small Angle X-Ray Scattering and Wide Angle X-Ray Scattering (SAXS/WAXS) Measurements at Ambient Temperature. SAXS and WAXS samples with a 0.5 mm thickness were prepared by compression moulding at 290 °C and then cooled down to room temperature at a 20 °C/min rate. SAXS and WAXS were performed under vacuum at room temperature on rectangular bars using a Xeuss 2.0 SAXS/WAXS system (Xenocs SA, France). Cu K-α radiation (GeniX3D Cu ULD, λ = 1.54 Å, 50 kV, 0.6 mA) was generated. A semiconductor detector (Pilatus 300K, 487×619 pixel resolution, DECTRIS,

Switzerland) was used to collect the scattering signals. Each sample was exposed under X-ray for 20 min. All data were corrected by background and empty beam scattering.

Simultaneous SAXS/WAXS Synchrotron Measurements. The structural evolution during heating and cooling was followed in-situ by WAXS and SAXS using synchrotron radiation at the ALBA Synchrotron radiation facility (beamline BL11-NCD) in Cerdanyola del Vallés, Barcelona, Spain. The samples were placed in a Linkam hot stage (THMS-600 model) that was linked with a liquid nitrogen cooling equipment. All samples were cooled down from the melt (280 ºC) to 100 ºC at a 20 ºC/min cooling rate and then heated up to 280 ºC at 20 ºC/min heating rate. WAXS/SAXS measurements were taken regularly every 30 seconds during both cooling and heating runs. The X-ray source employed had an energy of 12.4 keV with $\lambda = 1.0$ Å. A Rayonix LX255-HS detector was employed for the WAXS configuration, with a 230.4×76.8 mm^2 active image area, a 44 μm^2 pixel size, and a 15.5 mm distance (tilt angle = 27.3°). The sample detector (Pilatus 1M) for the SAXS mesurments had an 168.7×179.4 mm^2 activate image area, a 981×1043 total number of pixels, a 172×172 μm^2 pixels size, a 25 frames/sec rate, and a 6463 mm distance. The calibration of the scattering vector was accompulished by means of silver behenate (for SAXS experiment) and chromium (III) oxide (for WAXS experiment).

Dynamic Mechanical Thermal Analysis (DMTA). The phase behaviour of the blend samples was investigated by DMTA using a TA Q-800 viscoelastometer. Scans were performed at 4 °C/min heating rate from -100 °C to 150 °C using a single cantilever bending mode with a frequency of 1 Hz.

Density. Density measurements were performed using a electronic densitometer (Mirage SD-120L) and n-butanol was used as immersion liquid. For each reported value,

two impact specimens were weighed and the temperature of the immersion liquid was determined (with 0.1 °C precision).

Birefringence. The global orientation of the materials was measured by means of birefringence, which was determined in a prism coupler (Metricon model 2010) fitted with an infrared laser operating at 1550 nm wavelength. The measurements were carried out at three points on the surface of the central part in tensile samples, which were cut with a Leica 1600 microtome.

Mechanical Properties. Tensile tests of dumbbel samples were performed with a universal testing equipment (Instron 5569, Norwood, USA). Young's moduli were determined with the help of an extensometer and a strain rate of 1 mm/min. Tensile strength (σ_t) and breaking strain (ε_b), were obtained from the load-displacement curves using a crosshead speed of 1 cm/min. At least five tensile samples were examined for each reported value. Impact tests were measured (Ceast pendulum, ASTM D-256) on the injection moulded specimens with a cross section of 12.7×3.2 mm. Notches were machined in the injection molded bars with a depth of 2.54 mm and a radius of 0.25 mm. At least eight samples were tested to determine the average impact strenght.

RESULTS AND DISCUSSION

Differential Scanning Calorimetry (DSC)

DSC scans of the neat polyamides and the PA6/PA410 blends are presented in Figure 1. Neat PA410 crystallizes and melts at higher temperatures than neat PA6. The DSC cooling scans are presented in Figure 1a with close ups of certain blend compositions in Figure 1b. Samples in Figure 1a and 1b were cooled from the melt at 20 °C/min. For each blend, two sets of DSC curves are presented. The curves plotted in thin black lines

correspond to "unmixed blends". These curves are the weighted average DSC traces of the homopolymer and represent the DSC curves that would be obtained if there were no interactions between the blend components. It can be appreciated that these "unmixed" blends traces are quite different from the DSC cooling scans of the real melt mixed blends.

The 10/90 and 20/80 PA6/PA410 blends exhibit a single crystallization temperature, T_{c1}, which corresponds to the crystallization temperature of the PA410 rich phase, as judged by comparison with the "unmixed blends" DSC scans. The blends with 70 wt % PA410 or less showed two separate crystallization peaks, of which the higher temperature one corresponds to the PA410 rich (T_{c1}) and the lower temperature one (T_{c2}), to the PA6 rich phase crystallization.

In the close up presented in Figure 1b, the total absence of the PA6 rich phase crystallization for the 10/90 and 20/80 PA6/PA410 blends can be appreciated, especially when the cooling DSC scans are compared with those of the unmixed blends. The crystallization of the PA410 rich phase in Figure 1b is always observed with a very clear exothermic peak that appears at temperatures lower than those in the "unmixed blends".

The crystallization of the PA6 rich phase is very clear in Figure 1a for blends with 90 to 50 % PA6 content. Figure 1b shows that when the content of PA6 falls below 50%, the PA6 rich phase crystallization is more subtle. For the 40/60 PA6/PA410 blend, a broad exothermic peak at around 185 ºC can be observed in contrast with the sharp expected peak illustrated by the unmixed 40/60 PA6/PA410 blend (see Figure 1b). For the 30/70 PA6/PA410 blend, the crystallization of the PA6 rich phase is even more difficult to see with the employed scale, as it is very broad and exhibits a much smaller crystallization enthalpy in comparison with the unmixed blend. For the 20/80 and 10/90 PA6/PA410

blends, no crystallization of the PA6 rich phase could be detected, in contrast with the sharp exothermic signals present in the unmixed blends at around 183 ºC.

Figures 1c and 1d show the subsequent heating DSC scans after the cooling runs presented in Figures 1a and 1b. The melting data is consistent with the presence of a single crystalline phase formed by the PA410 rich phase (with possible PA6 chains incorporated inside the PA410 crystals) for the case of the 10/90 and 20/80 PA6/PA410 blends. The corresponding unmixed blends show that bimodal melting could have been observed, if the PA6 phase would have crystallized. For the blends containing 70 wt% PA410 or less, two melting points associated with the PA410 rich and the PA6 rich phases can be clearly observed (Figure 1c). However, comparing with the unmixed blends, Figure 1d qualitatively shows (as will be also quantitatively demonstrated in Table 2 below) that the amount of PA6 rich crystals that melt in the melt mixed blends is lower than the value theoretically expected for the 30/70 and the 40/60 PA6/PA410 blends (as indicated by the comparison with the unmixed blends melting curves).
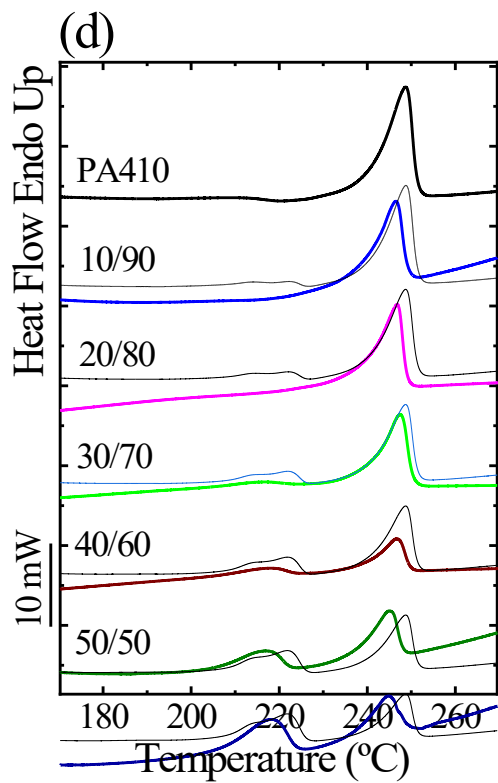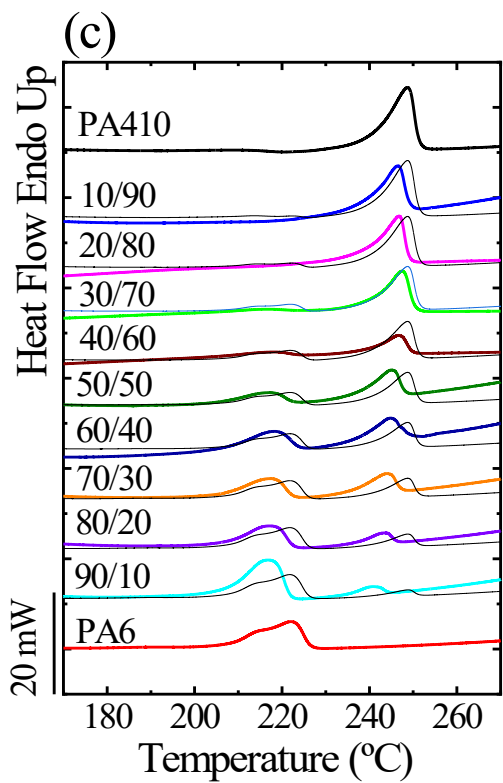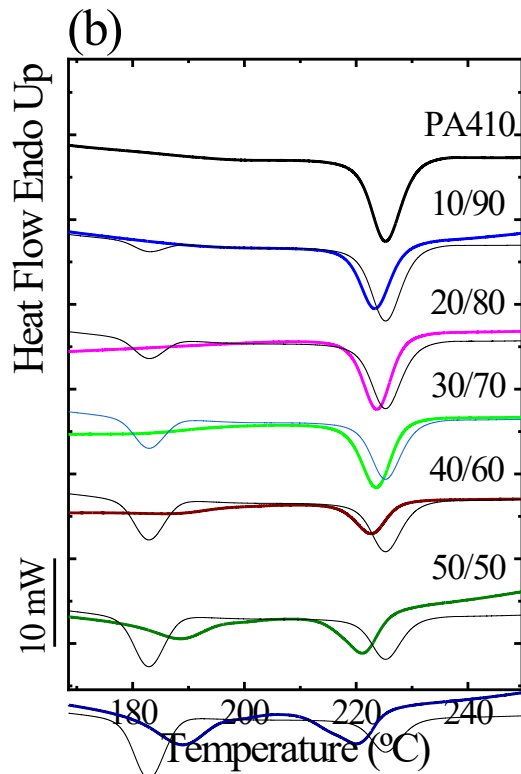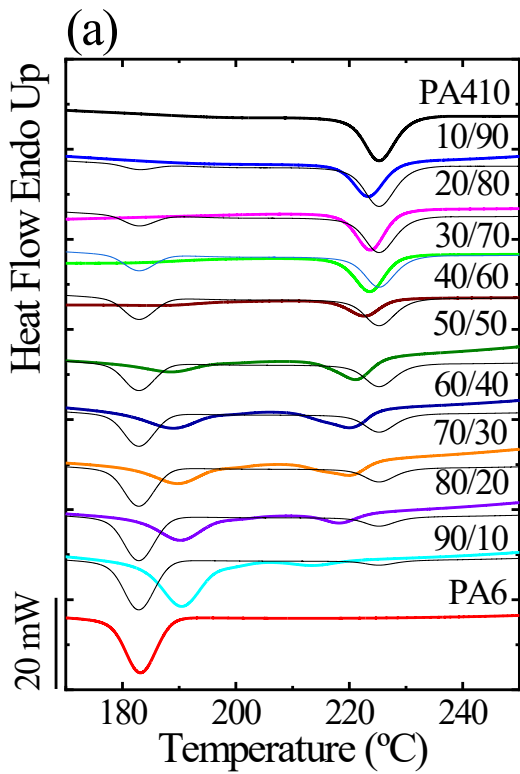
Figure 1. DSC scans of PA6/PA410 blends (a,b) cooling runs (c,d) 2nd heating runs at 20 ºC/min rate. The blend composition (wt. %) is indicated by the numbers above the curves.

Taking into account the results of Figure 1, we realize that as PA6 is added to PA410, first a single crystalline phase (where both chains most probably co-crystallize, see also WAXS evidence presented below) is formed (i.e., 10/90 and 20/80 PA6/PA410 blends) and then for 30 and 40% of PA6, phase separation occurs during crystallization, but still part of the PA6 chains co-crystallize with PA410, depleting the amount of the PA6 rich phase that can crystallize and melt at lower temperatures. Finally, with addition of 50% of PA6 or more to PA410, the phase segregation during crystallization is more extensive, as the enhalpies of crystallization and fusion approach the values displayed by the unmixed blends. Table 1 specifies the data from the cooling and the second heating runs of the non-isothermal DSC runs for PA6/PA410 blends, neat PA6, and neat PA410.

Table 1. Data extracted from the cooling and second heating scan of the non-isothermal DSC run at a 20 ºC/min scan rate.

Polyamide compositions PA6/PA410	Cooling Run				Second Heating Run			
	T_{c1} (°C)	ΔH_{c1} (J/g)	T_{c2} (°C)	ΔH_{c2} (J/g)	T_{m1} (°C)	ΔH_{m1} (J/g)	T_{m2} (°C)	ΔH_{m2} (J/g)
0/100	225.0	53	-	-	248.3	59	-	-
10/90	223.5	51	-	-	246.4	57	-	-
20/80	223.5	49	-	-	246.4	55	-	-
30/70	223.5	45	183.1	5	246.4	44	216.7	4
40/60	222.6	40	186.1	10	246.4	38	216.7	8
50/50	221.1	32	188.9	18	244.9	31	216.7	15
60/40	219.8	25	189.1	24	244.9	24	216.7	20

70/30	219.8	15	190.1	29	243.9	15	216.7	27
80/20	218.5	9	190.1	35	243.1	9	216.7	32
90/10	213.4	4	190.2	48	240.6	3	216.7	42
100/0	-	-	182.9	54	-	-	220.0	48

* Subscript 1 indicates PA410 rich phase and subscript 2 indicates PA6 rich phase.

The DSC cooling runs in Figure 1 showed that the two neat polyamides crystallized in different, well-separated temperature regimes. According to Figure 2a, T_{c1} values (the T_c of neat PA410 and PA410 rich phase in the blends) progressively shift to lower temperatures as the PA6 content increases. On the other hand, the crystallization temperature of the PA6 rich phase (T_{c2}) of the blends increases when 10% PA410 is added and then gradually decreased. This is caused by a nucleation effect of the PA410 rich phase crystals on the PA6 rich phase crystals.

Figure 2b shows that the T_{m1} value (corresponding to the PA410 rich phase crystals) of the blends decreases with increasing PA6 content. A large part of the PA6 component in the blends is molten at the temperatures at which the PA410 rich phase crystals melt and this probably causes a diluent effect that depresses the melting point of these crystals [58]. On the other hand, all the PA6 rich phase crystals in the blends exhibit a constant melting point that is a few degrees lower than the T_m of neat PA6. The shaded region in Figures 2a and 2b indicate the blends that contain only one type of crystals for those compositions, i.e., the PA410 rich phase crystals (or co-crystals of PA410 with some PA6 chains).

We also measured the equilibrium melting point T_m^0 by performing isothermal crystallization measurements at high temperatures, where the PA410 phase crystallizes, and then we immediately heated the sample to record the melting point. We then used the

Figure 2b also shows the glass transition temperature (T_g) values obtained by DMTA for all the PA6/PA410 blend compositions. As shown, all blend compositions display a single glass transition temperature, which is the usual criterion to deduce miscibility in the amorphous phase [25, 60-65]. Moreover, the values are intermediate between those of the neat components, decreasing linearly as the PA6 content increased and thus, following the Fox equation for miscible blends [66]. For this kind of self-associated polyamide blends, usually, transamidation improves the miscibility between blend components in the melt and in the amorphous state. Similar results have been obtained for PA6/PA6I-*co*-T (PA6/ semiaromatic amorphous polyamide)blends [25, 60-62].

In Figure 2c, the enthalpy of fusion, ΔH_m, obtained from the area under the melting peaks of the DSC curves in Figure 1b, is plotted *versus* composition. ΔH_{m1} and ΔH_{m2} values were normalized with respect to the content of PA410 and PA6 in the blends, respectively. ΔH_{total} values of the blends are calculated using $\Delta H_{total} = \Delta H_{m1} + \Delta H_{m2}$ and they are lower than those of neat PAs. As shown in Figure 2c, both ΔH_{m1} and ΔH_{m2} decreased as the second component in the blend increases.

The results presented in Figures 1 and 2 show that only PA410 rich phase crystals are formed up to a certain composition (i.e., 20% PA6), beyond which phase segregation during crystallization is triggered and two crystalline phases are formed by the blend (i.e., a PA410 rich crystalline phase and a PA6 rich crystalline phase). We assume that the blends

are forming a single phase in the melt. This is a reasonable assumption, as the blends are miscible in the amorphous state, as indicated by their single T_g over the entire composition range. On the other hand, SAXS data collected in the molten state do not show any scattering signal that could indicate the presence of two phases. Either the blends form a single phase in the melt, or the scattering contrast is too weak to show differences between the phases. Furthermore, phase contrast microscopy experiments in the melt (not shown here) indicate a homogeneous melt within the microscopic scale of the observation of the optical microscope. SEM observations were also made in cryogenically fractured specimens and there were no evidences of phase segregation in the obtained morphology. It is possible that the contrast between the two phases is not enough to reveal any difference between the phases, but we were not able to find any proof of phase segregation in the melt by SAXS, SEM or optical microscopy.
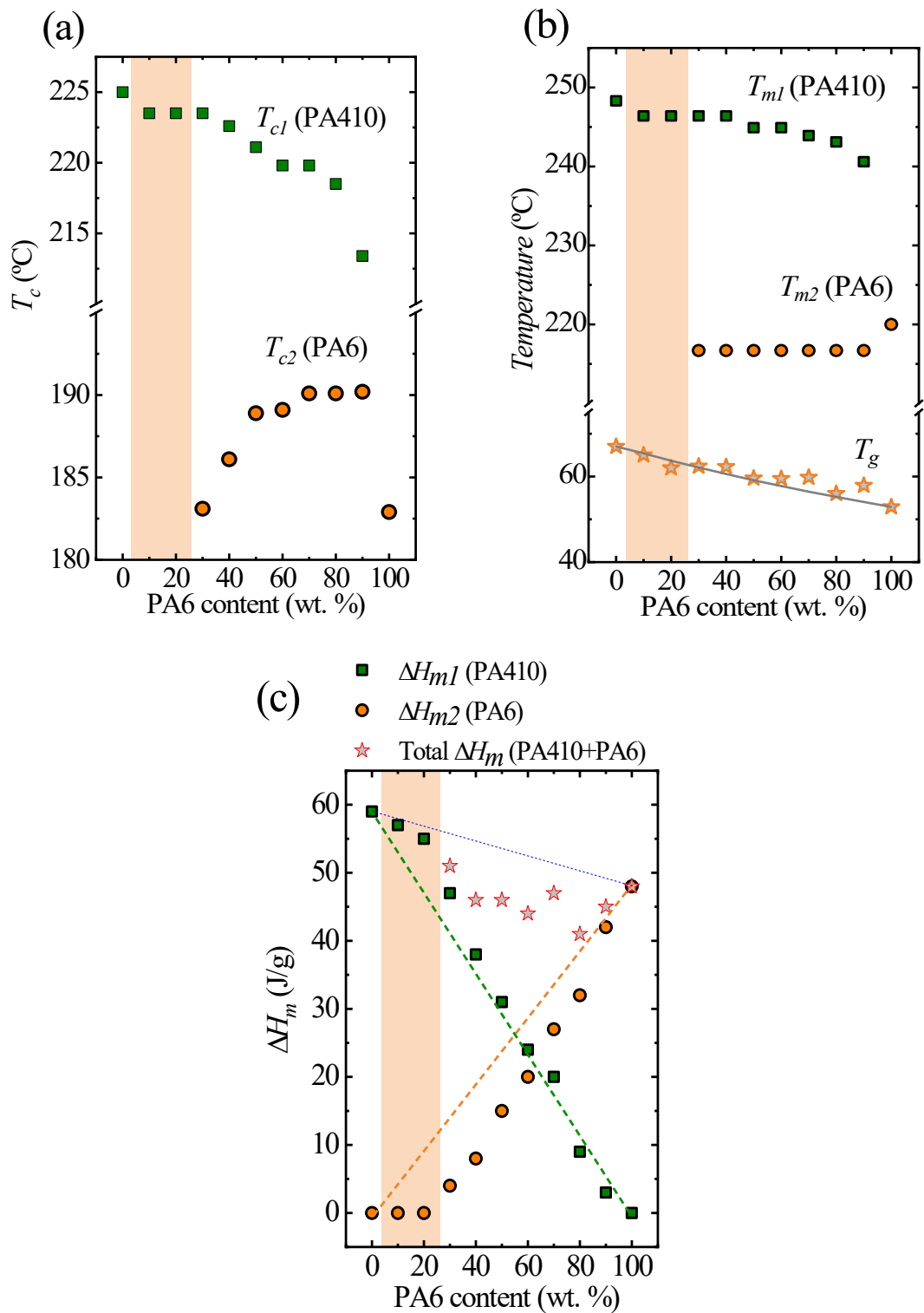
Figure 2. (a) Crystallization temperature T_c; (b) Melting temperature T_m and glass transition temperature T_g; (c) Melting enthalpy ΔH_m for the indicated samples as a function

of PA6 composition. The shadowed region denotes the blends that form a single crystalline phase (i.e., a PA410 rich crystalline phase).

In summary, the 10/90 and 20/80 PA6/PA410 blends form a single PA410 rich crystalline phase, with unique T_c and T_m values. For blends with 30 % PA6 or more, crystallization driven phase segregation occurs, and the blends become double crystalline with coexisting PA410 rich and PA6 rich crystalline phases. The amorphous phase is always miscible, as a single T_g is observed in the entire composition range.

The contribution of each polyamide component within the crystalline phase of the other component was roughly estimated by normalization of the experimental ΔH_m values, using their weight fraction and by comparing these experimental values with the expected theoretical ones (i.e., using a simple rule of mixtures). We have calculated the incorporation of PA6 chains inside the PA410 crystals in this way, as an approximation.

As can be seen in Table 2, by increasing the PA6 content in the blend, the incorporation of PA6 chains in the crystalline phase of PA410 decreased. For instance, the incorporation of PA6 chains within the PA410 rich crystalline phase is about 83% for the blend with 10% PA6, whereas it decreased to 4% for the blend with 50% PA6. Higher amounts of PA6 (more than 50%) seems to facilitate phase separation and prevent the incorporation of any significant amount of PA6 chains within the PA410 rich crystalline phase; as judged by the changes in enthalpy of melting. This behavior can be rationalized by looking at Figure 2c where the enthalpies of melting are plotted. The normalized enthalpy of melting for the PA410 rich crystalline phase (i.e., ΔH_{m1}) has a positive deviation from a linear rule of mixtures for those blends rich in PA410 and the highest positive deviations are observed for the 10/90 and 20/80 PA6/PA410 compositions (where

a single crystalline phase was formed, as indicated by the shadowed region in the figure).

As expected, the normalized enthalpy of melting for the PA6 rich crystalline phase (i.e.,

ΔH_{m2}) exhibits a negative deviation from a linear rule of mixtures, as PA6 chains tend to be

incorporated within the PA410 rich crystalline phase, therefore depleting the amount of

PA6 rich crystalline phase.

Table 2. Incorporation of PA6 in PA410 crystals calculated by using the changes in enthalpies of the blends

PA6 (% wt.)	Theoretical ΔH_{m1} (J/g)	Theoretical ΔH_{m2} (J/g)	Experimental ΔH_{m1} (J/g)	Experimental ΔH_{m2} (J/g)	PA6 incorporation (%)
0	59	0	59	0	-
10	53	4.8	57	0	83
20	47	10	55	0	80
30	41	14	44	4	21
40	35	19	38	8	16
50	30	24	31	15	4
60	24	29	24	20	0
70	18	34	15	27	0
80	12	38	9	32	0
90	6	43	3	42	0
100	0	48	0	48	-

* Subscript 1 indicates PA410 and subscript 2 indicates PA6.

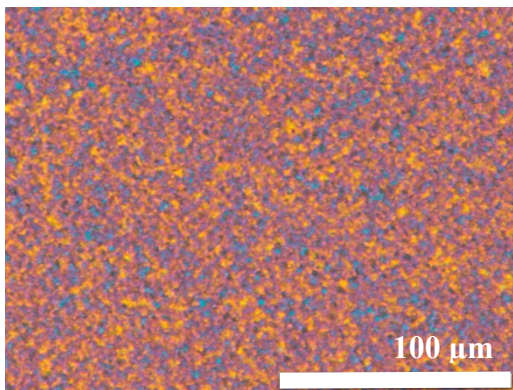**Polarized Light Optical Microscopy (PLOM)**

PLOM was used to visually study blend morphology and detect differences in the

spherulites morphology of the samples. PLOM images were recorded after non-isothermal

crystallization from the melt (see Figure SI-1). Both neat PA410 and PA6 exhibit a microspherulitic morphology that prevented any measurement of growth rates as the nucleation density was always too large. However, we were able to detect the presence of one or two crystalline phases by the changes experienced by the birefringence during crystallization.

Figures 3a and 3b show PLOM micrographs of the 20/80 PA6/PA410 blend that forms a single crystalline phase (corresponding to a PA410 rich crystalline phase), according to the DSC results (see Figure 1). The microspherulitic texture was seen forming at 230 ºC (a temperature at which the PA6 chains are in the melt or co-crystallizing with PA410), further cooling caused no significant changes in the morphology, as seen in the PLOM micrograph captured after the sample was cooled down to 180 ºC and held at that temperature for 5 min.

On the other hand, the mirror composition sample, i.e., 80/20 PA6/PA410 blend, is capable of forming two separate crystalline phases upon cooling from the melt according to Figure 1. This is corroborated in Figures 3c and 3d, where PLOM micrographs are shown. First, the sample was cooled from the melt and crystallized at 230 ºC for 5 min, durig which the PA410 rich crystalline phase formed microscopic spherulites. Then, the sample was cooled to 180 ºC and kept at that temperature during 5 min, during which the PA6 rich crystalline phase was formed. The obvious change in birefringence between Figure 3c and 3d is a strong evidence for the second PA6 rich phase formation (as are the DSC scans presented in Figure 1).
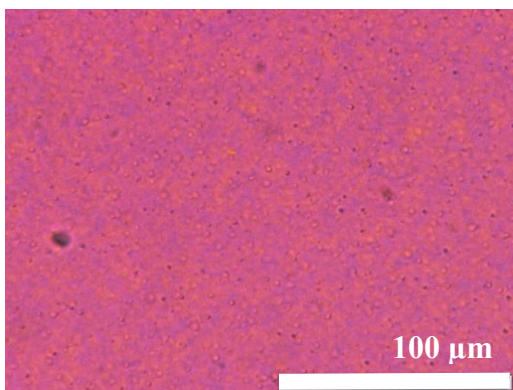
(a) 20/80 (*after 5 min at 230 °C*) (b) 20/80 (*after 5 min at 180 °C*)
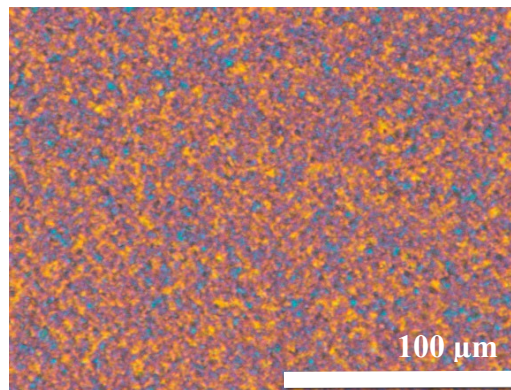
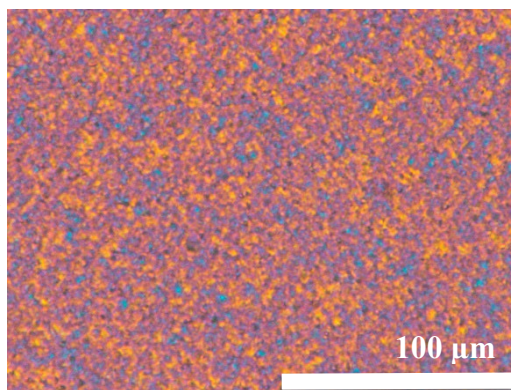(c) 80/20 (*after 5 min at 230 °C*) (d) 80/20 (*after 5 min at 180 °C*)

Figure 3. PLOM micrographs for: (a) the 20/80 PA6/PA410 blend after it was first melted at 270 ºC/min to erase any preserved thermal history and then quenched to 230 ºC, where it was allowed to crystallize for 5 min; (b) same sample as in (a) after it was quenched to 180 ºC and kept at that temperature for 5 min; (c) the 80/20 PA6/PA410 blend after it was first melted at 270 ºC/min to erase thermal history and then quenched to 230 ºC, where it was allowed to crystallize for 5 min; (d) same sample as in (c) after it was quenched to 180 ºC and held at that temperature for 5 min.

SAXS and WAXS Study at Room Temperature

Figure 4a shows the results from Wide-Angle X-ray Scattering (WAXS) of neat PA6, neat PA410, and their blends. Neat PA6 shows two characteristic peaks at $q_1 = 14.22$ and $q_2 = 16.77$ nm^{-1}, which are assigned to the (200) and (002/220) plane reflections of the α-form [59], which has a monoclinic unit cell with $a = 0.956$ nm, $b = 1.724$ nm (chain axis), $c = 0.801$ nm, $\beta = 67.5°$. PA410 shows two well defined intense peaks located at $q_1 = 14.30$ and $q_2 = 16.70$ nm^{-1} (allocated to the (100) and (010/110) plane reflections) and a small peak at 4.04 nm^{-1} assigned to (001) plane. The unit cell parameters of PA410 are: $a = 0.490$ nm, $b = 0.532$ nm, $c = 1.98$ nm (chain axis), $\alpha = 49°$, $\beta = 77°$ and $\gamma = 63°$ [63] (note that the definition of chain axis are different for the two polymers). The most intense crystalline reflections overlap and make the distinction between the two types of crystals very difficult. Figure 4b shows the *d*-spacing evaluated from the peak positions of the WAXS patterns for these blend samples. The *d*-spacings barely showed any change with composition. Although the two main reflection peaks of polyamides are overlapped, it is possible to detect the presence of PA410 crystals in the blends through a small peak at $q = 4.04$ nm^{-1} which corresponds to the (001) plane.

A clear difference between the two polyamides is the intensity ratio of the two main peaks: Iq_1 / Iq_2. For PA6 and PA410, the intensity ratios are 1.15 and 2.73, respectively. Figure SI-2 shows an example of the extraction method used to calculate the intensity ratio values from WAXS patterns.
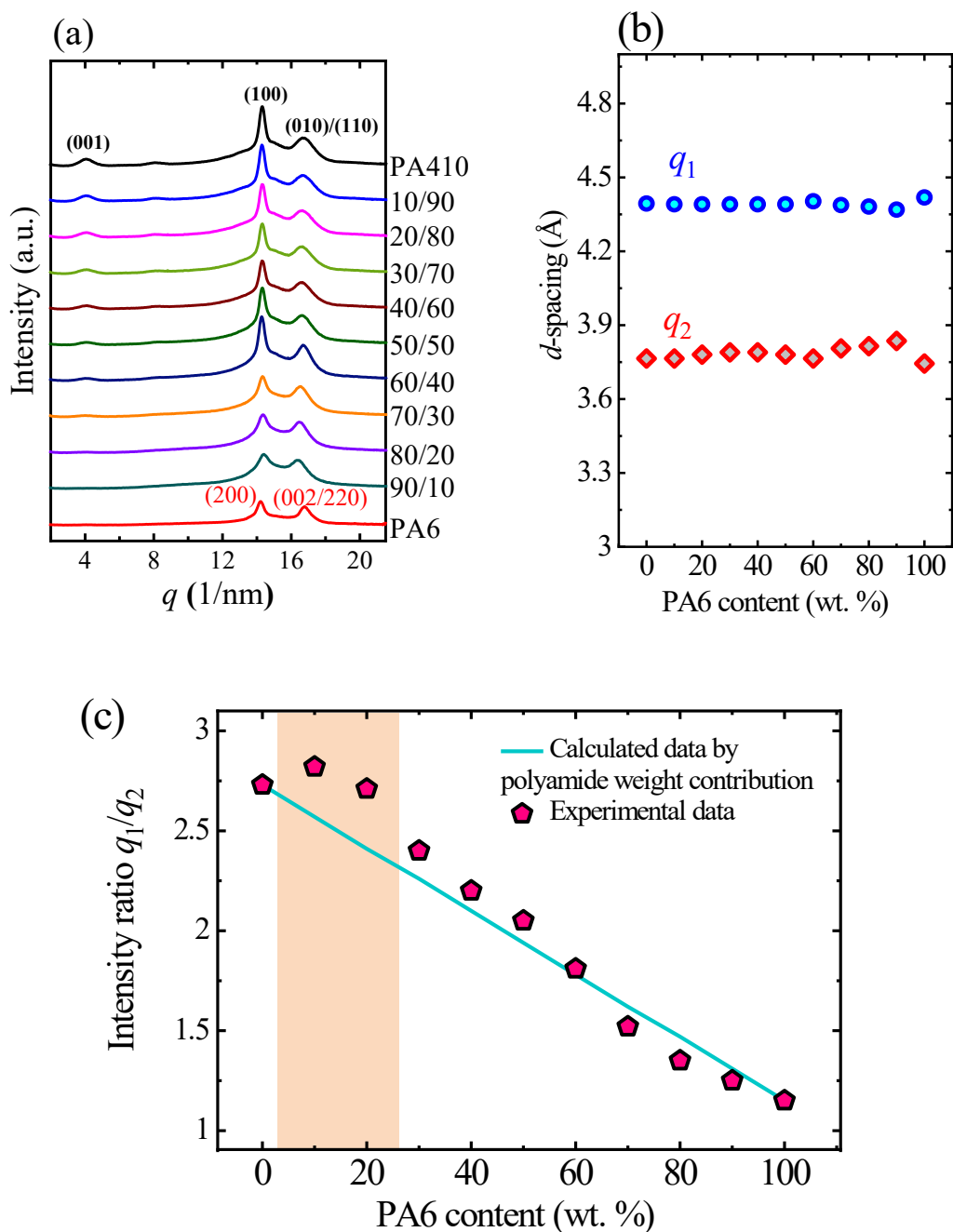
Figure 4. (a) WAXS patterns of all PA6/PA410 blend samples at room temperature. (b) *d*-spacing changes *versus* PA6 content. (c) Changes in intensity ratio of the two main peaks, q_1 and q_2, in PA6/PA410 blends *versus* PA6 content. The shadowed region denotes the blends that form a single crystalline phase (i.e., a PA410 rich crystalline phase).

The ratio of these peaks *versus* PA6 content is plotted in Figure 4c. If the blend samples followed a simple mixing rule without any change of each individual component, the intensity ratio of these peaks would be an average of the two peaks based on their weight contribution (black line in Figure 4c). However, it can be seen that the experimental data (pink pentagons in Figure 4c) showed a clear positive deviation from a simple rule of mixtures for compositions with less than 50 % PA6.

As mentioned in the DSC section, the blend samples with less than 50% PA6 showed calorimetric signs of incorporation of PA6 chains into the PA410 rich phase crystals (see Table 2). These changes in the intensity ratio of the two main peaks with the composition are additional evidence of the incorporation of PA6 chains in the PA410 rich crystal phase for blends with less than 50 % PA6. In particular, the maximum positive deviation from a rule of mixtures is observed for the two blends (i.e., the 10/90 and 20/80 PA6/PA410 blends) that contain only a single crystalline phase as evidenced by DSC (a PA410 rich crystalline phase); they are highlighted by the shaded region in Figure 4c.

SAXS patterns of neat polyamides and all blend samples at 25 ºC are shown in Figure 5a. Surprisingly, all samples exhibited a single peak that can be interpreted as the scattering attributable to lamellar stacks, and the long periods (L_p) were calculated from the q_{max} values after Lorentz correction by Equation 1.

$$L_p = \frac{2\pi}{q_{max}} \qquad \text{Eq (1)}$$

SAXS patterns in Figure 5a exhibited a single peak corresponding to lamellar packing of about 7.5-10.0 nm depending on blend composition. Figure 5b presents the changes in the long period (L_p) as a function of PA6 content. In the 0-60% PA6 range, L_p

first increased then remained constant when adding PA6. In intermediate compositions, the sample is expected to have a multiphasic microstructure containing crystalline PA6 rich lamellae, crystalline PA410 rich lamellae and amorphous phase. The electron density of the crystalline phase of PA6 and PA410 can be estimated by the density of unit cells, which is 1.23 g/cm^3 for PA6 and 1.22 g/cm^3 for PA410. A simple calculation indicates that the electron density of the crystalline phase for PA6 and PA410 is coincidenctly the same (406 e/nm^3). Therefore, there is no scattering contrast between the crystalline PA410 and PA6 phase.
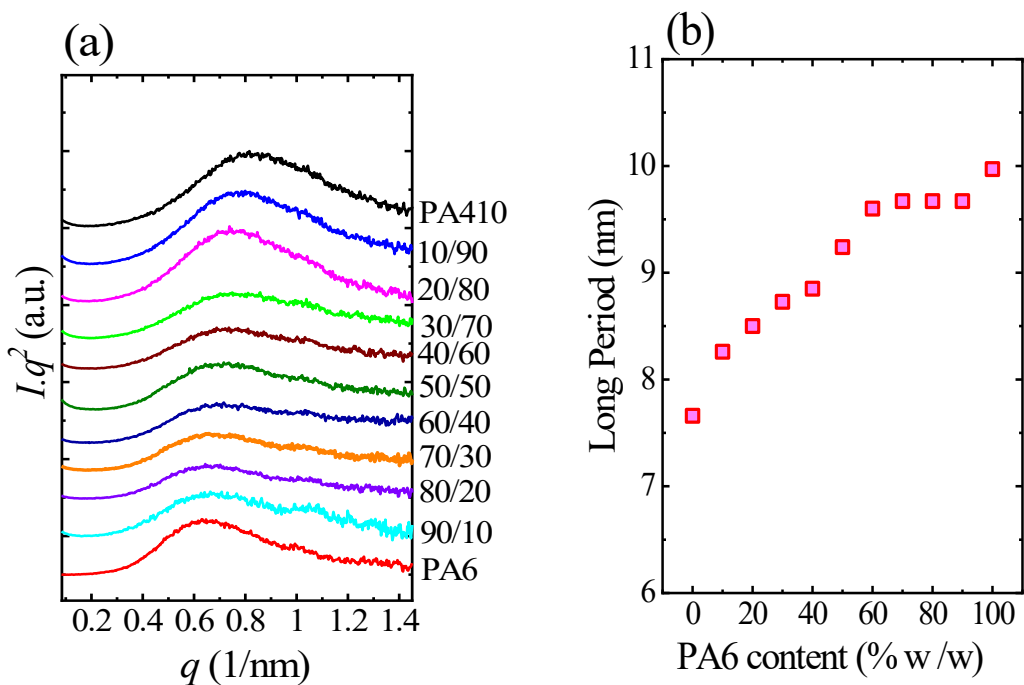

Figure 5. (a) SAXS diffraction patterns of neat PA410, neat PA6, and PA6/PA410 blends registered at 25 ºC. Inserted numbers indicate PA6/PA410 wt. %. (b) Changes in long period values *versus* PA6 content calculated from SAXS diffraction.

The single peak in SAXS curves can be explained as the average period of the lamellar packing in the samples. The change of L_p with composition may indicate the

existance of two types of microstructures. For example, in the PA410-rich region (left side of Figure 5b), it is possible that the uncrystallized PA6 is mainly incorporated in the interlamellar amorphous region of PA410 except for a the fraction that is included in the crystalline phase (see Table 2). This will result in a thicker amorphous layer and therefore a thicker long period. On the other hand, in the PA6 rich region, the long period changed little possibly because of the strong tendency of crystallization driven phase separation.

In-situ WAXS and SAXS

In-situ non-isothermal crystallization experiments were carried out for four selected compositions using synchrotron radiation. Selected WAXS patterns of the 60/40 PA6/PA410 blend during cooling and heating are shown in Figure 6a and 6b, respectively. The intensity of the crystalline reflections increased with decreasing temperature. WAXS patterns during the cooling and heating of neat PA6, neat PA410, and 20/80 blends are shown in Figure SI-3.

Figure 6c shows the changes in the intensity ratios of the two main reflections of polyamides (Iq_1/Iq_2) as a function of temperature during the cooling run for selected samples. Here, we studied the neat polyamides, the 20/80 composition (which shows the incorporation of PA6 chains within the PA410 rich crystalline phase), and the 60/40 composition (which shows two separate crystalline structures). In the case of 60/40 blend (green line), where a total crystalline phase separation occurs, the intensity ratio jumps to lower values at the temperature at which PA6 starts crystallizing. Therefore, both types of crystalline phases can form separately in the 60/40 composition (i.e., a PA6 rich crystalline phase and a PA410 rich crystalline phase), as phase segregation is driven by crystallization. However, the sample with 20% PA6 did not show (see Figure 6c) any abrupt change in the

temperature range where the PA6 rich phase typically crystallizes in the blends (indicating

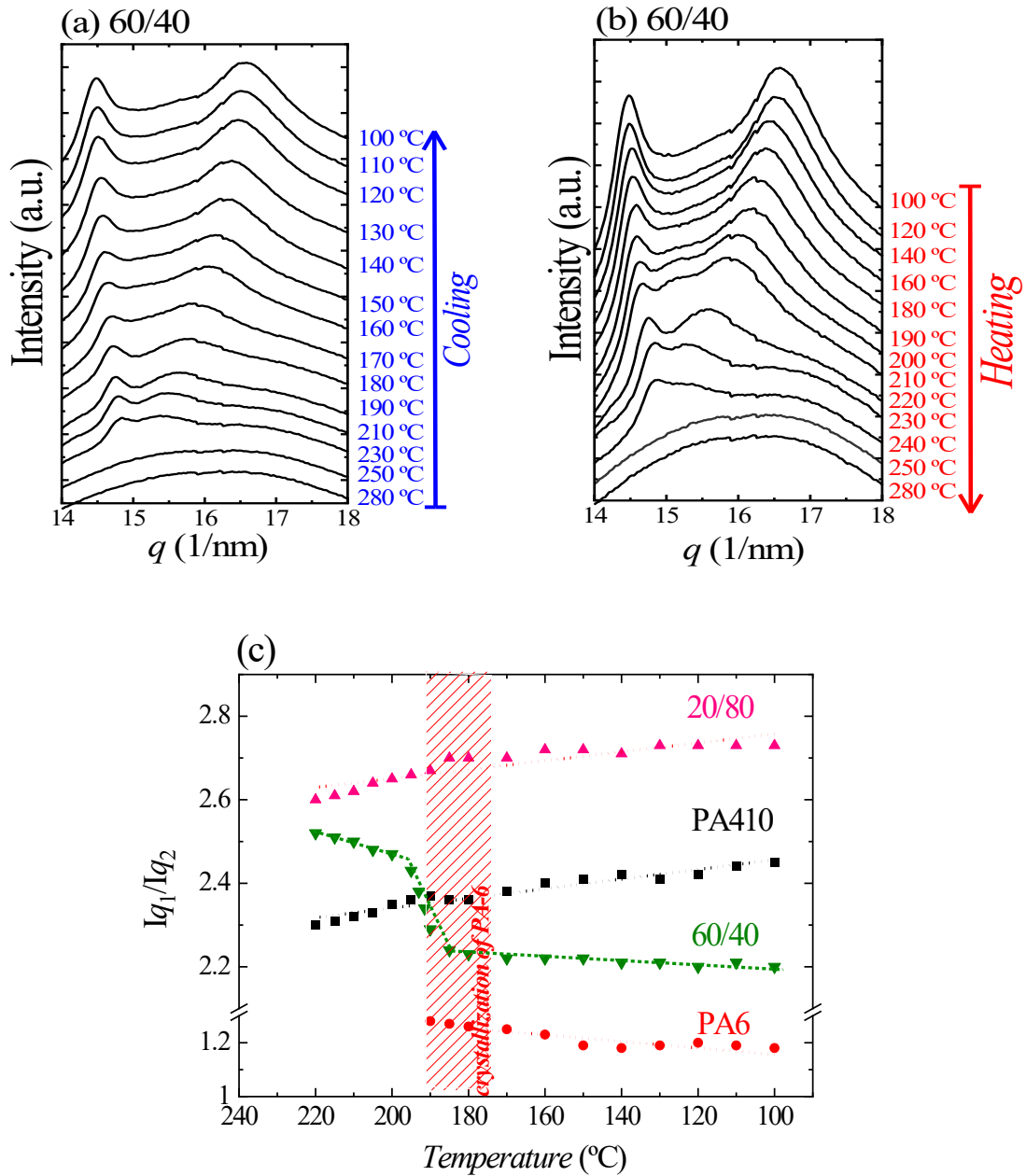co-crystallization of PA6 inside the PA410 rich crystals).

Figure 6. In-situ WAXS patterns of the 60/40 PA6/PA410 blend during the cooling (a) and heating (b) process at the indicated temperatures. Data extracted from WAXS scattering during cooling run at a 20 ºC/min cooling rate for the indicated samples (c).

In-situ SAXS measurements were also carried out during non-isothermal crystallization experiments for the four selected compositions using synchrotron radiation to further understand the morphology of the blends. As an example, Figure 7a show the temperature-dependent SAXS patterns measured for the 60/40 PA6/PA410 blend during the cooling from the melt at 20 ºC/min cooling rate. The SAXS patterns during heating the 60/40 PA6/PA410 blend (Figure SI-4 g), as well as the SAXS patterns during heating and cooling for for the other 3 samples are shown in Figure SI-4 a-f.
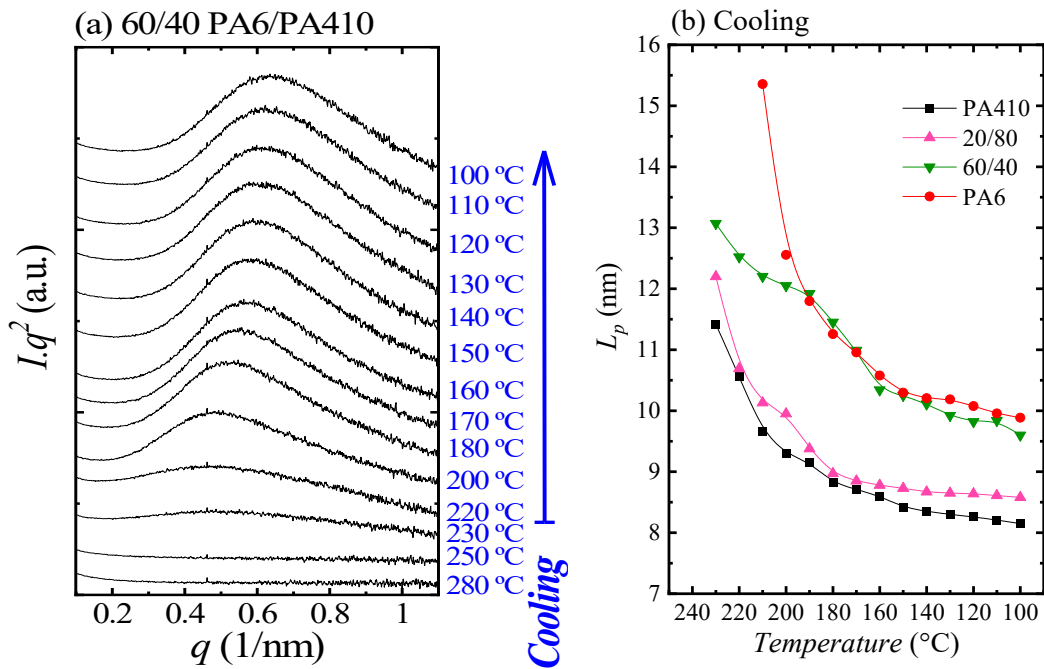

Figure 7. In-situ SAXS diffraction patterns of 60/40 PA6/PA410 registered during (a) the cooling run (from 280 ºC to 100 ºC) and (b) the long period of several samples during cooling as a function of temperature.

DSC results confirmed (Figures 1 and 2) that the 60/40 PA6/PA410 blend showed two separate values of T_m and T_c. Figure 7a shows that no SAXS signal can be seen in the melt and a single peak appears during cooling. The long period value of the four samples as

a function of temperature during cooling and heating are plotted in Figure 7b and Figure SI-5, respectively. Interestingly, the 20/80 PA6/PA410 sample shows very similar long period values to the neat PA410. However, the 60/40 PA6/PA410 shows a two-step change during cooling which agrees well with the separate crystallization of the two components.

In Figure SI-6, the long period values are plotted as a function of PA6 composition at 210 ℃, where PA410 is in the crystalline state while PA6 is molten. It is clear that the L_p increases with the concentration of PA6, suggesting that the PA chains locate in between the crystalline lamellae of PA410. The results support the conclusion that the PA410 and PA6 are melt miscible.

In summary, both in situ WAXS (Figure 6) and SAXS (Figure 7) were able to show the formation of one (for the 20/80 PA6/PA410 blend) or two crystalline phases (for the 60/40 PA6/PA410 blend) upon cooling from the melt depending on the blend composition. The results agree well with those obtained by DSC (Figure 1 and Table 2).

Miscibility of polyamides strongly depends on the chemical structure of blended polyamides and their polymeric interactions, in particular the hydrogen bonding between the different chains [67]. According to the chemical structures of PA6 and PA410 (see Figure SI-7), hydrogen bonds between their chains are easily formed, despite a small distance between N-H and C=O groups in the middle of the blend structure. Therefore, the amorphous parts of PA6 and PA410 are miscible possibly due to the similarity of their chemical structures.

Mechanical properties

Table 3 shows the tensile and impact properties of PA6/PA410 blends over the whole range of compositions. Figures 8a-d show, respectively, the Young's modulus, tensile strength, ductility and impact strength of the blends *versus* the PA6 content.

As can be seen in Figure 8a, Young's modulus shows a slight synergistic behaviour over the whole range of compositions, as it remained unchanged with respect to that of the component with the higher value (PA410) up to the 70/30 PA6/PA410 composition (when standard deviations are considered), and decreased linearly at higher PA6 contents. Positive deviations in the modulus-composition relationship have often been observed in polymer blends. Although more common in miscible systems [68], partially miscible [68] and even immiscible blends have shown modulus synergism, when, for example, variations in orientation or crystallinity occur. As is well known, the basic condition for this behaviour is the compatibility between components, which is obviously assured in the case of the PA6/PA410 blends prepared in this work.

Table 3. Young's modulus, tensile strength, ductility and impact strength values of PA6/PA410 blends.

PA6/PA410	Young's modulus (MPa)	Tensile strength (MPa)	Strain at break (%)	Impact strength (J/m)
0/100	2860±60	81.6±0.3	41±11	35±1
10/90	2940±50	81.1±0.8	40±10	33±2
20/80	2930±40	79.7±1.1	37±27	33±1
30/70	2890±50	75.1±0.9	80±30	33±2

|			
40/60	2950±40	72.4±2.2	96±30	31±5
50/50	2930±40	73.4±2.5	129±51	33±2
60/40	2920±160	75.9±4.9	64±63	33±4
70/30	2800±180	72.7±5.9	118±75	36±1
80/20	2690±30	71.8±1.0	129±73	36±1
90/10	2610±30	70.0±0.7	108±66	41±2
100/0	2500±10	67.0±1.8	157±42	44±2

According to literature, there are three factors that can be different in the neat components and in the blends and, therefore, influence the Young's modulus: crystallinity [69-70], free volume [69-70] and orientation [69]. As discussed in previous sections, the blends showed crystalline contents below the linearity between the pure polyamides, showing a negative deviation from the rule of mixtures (Figure 2c). Therefore, this cannot be the cause of the observed positive modulus behaviour.

Possible blending-induced changes of the free volume were studied by means of density measurements. Figure SI-8 shows the density values of PA6/PA410 blends. As can be observed, the blends showed values that are intermediate between those of the pure components, with a slight positive deviation from the simple additivity rule. Similar results have been observed in several other works [69-74]. In this case, the 50/50 PA6/PA410 composition, for instance, shows a positive deviation of 0.002 g/cm^3 with respect to linearity (i.e., a 0.20 % increase). The same composition shows a positive deviation in the Young's modulus of 256 MPa (9.6 %). Vallejo and coworkers [70] observed comparable variations in specific volume and modulus for miscible PEI/PBT blends. In fact, they

attributed the modulus behaviour to the changes observed in the specific volume of the blends.

A possible change in the level of orientation of the blends with respect to the pure components was studied by means of birefringence measurements. Although the standard deviation and dispersion of the data obtained was high, a positive average deviation of 68% in birefringence was observed for all the compositions.

It is widely known that the level of orientation can affect the Young's modulus behaviour [69, 71]. As a consequence, injection moulded materials tend to show higher moduli than, for instance, compression moulded materials, as the former are usually more oriented [69, 71] and this, along with density, contributes to the positive deviation of modulus.
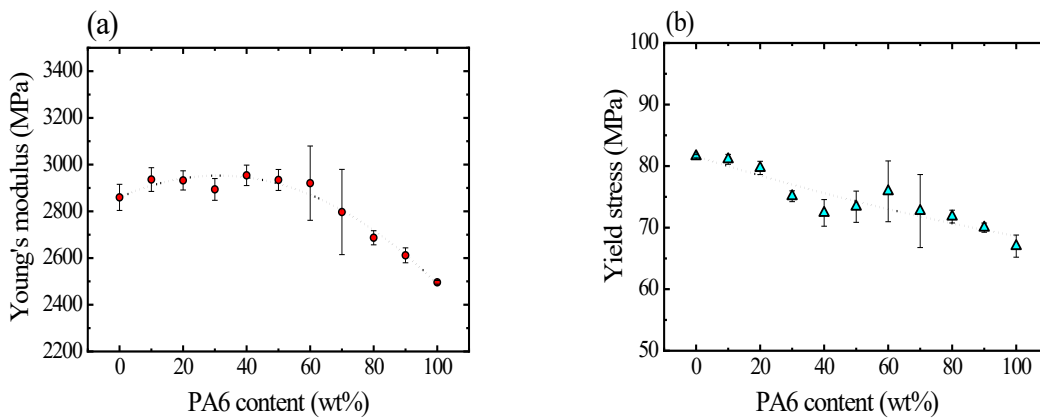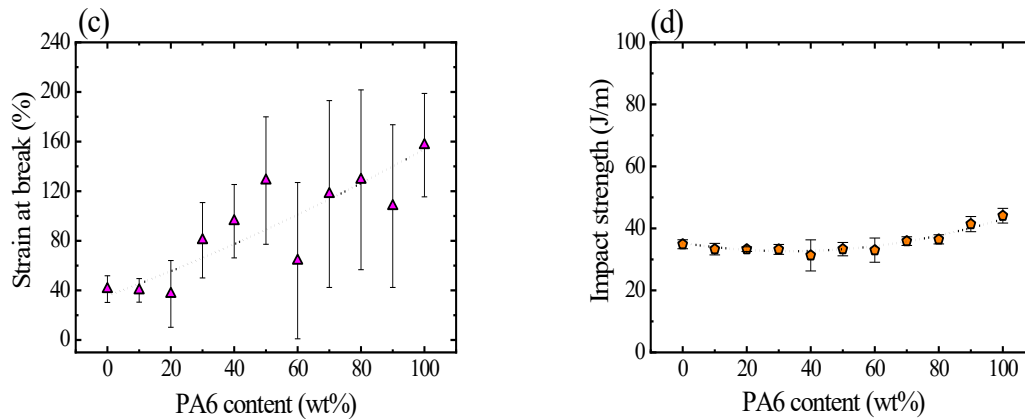
Figure 8. Young's modulus (a), yield stress (b), strain at break (c), and impact strength (d) of PA6/PA410 blends *versus* PA6 content.

These results point to the Young's modulus behaviour being affected by both the aforementioned negative deviation in the volume of mixing and the changes in the level of orientation in the blends with respect to the neat polyamides. However, it seems that the contribution of the former to Young's modulus is stronger than that of the latter, as the tendency observed in birefringence does not exactly fit that of the Young's modulus.

Figure 8b illustrates the yield stress values of the blends, which correspond to the tensile strength values in all cases. As can be seen, this parameter decreased as the concentration of PA6 in the blend increased, showing a performance close to linearity between the neat components. In previous works, it has been observed that the yield stress usually follows the same tendency as the Young's modulus [69-70]. However, examples of miscible systems in which the positive deviation observed in the Young's modulus is not reproduced in the yield stress [64] (and vice versa [71]) are also available in literature. As a matter of fact, miscible blends usually show a mechanical performance that is intermediate

34

between that of the neat components, as a consequence of the dispersion of the components at a molecular scale [69].

Figure 8c shows the strain at break values of the PA6/PA410 blends *versus* the PA6 content. As can be observed, all the compositions maintained the ductile nature of both neat components and values increased uniformly as the PA6 content increased, following the rule of mixtures. Although positive [65, 72-73, 75] and negative [68, 76] deviations have also been observed in literature, this is the usual behaviour in miscible blends [69, 77]. The standard deviations of the values of all the compositions were significantly high, probably because all the samples broke during the cold drawing process, which usually leads to high, though non-significant, scattering of the results obtained.

Figure 8d shows the impact strength values of the blends as a function of the PA6 content. As can be observed, both PAs and their blends show low impact resistance values, with a slight negative deviation from the simple rule of mixtures. This is because polyamides are very crack-sensitive materials [78-80]; hence, notched specimens show brittle fracture in high-speed deformation tests such as impact tests.

Negative deviations in impact resistance have often been observed in miscible polymer blends [18, 68, 70-73] and, in many cases [68, 70, 72-73], they have been attributed to the densification of the amorphous phase – more specifically, to the loss of free volume. Thus, it can be stated that in PA6/PA410 blends the positive deviation observed in the density is responsible for the impact strength behaviour.

Furthermore, in crack-sensitive materials such as nylons, it has been proposed [18] that the presence of weak points within the material (such as spherulite boundaries, nodes and

interlamellar regions[18], or even a partially miscible component [71]) could ease crack initiation and propagation, thus reducing the impact performance of the blends with respect to the one of pure components.

CONCLUSIONS

Blending offers an effective way of tuning the physical properties of polymers. In this work, we have systematically studied the miscibility, crystallization structure, morphology, and mechanical properties of PA410 and PA6 blends covering the entire composition range. The blends exhibited only one T_g in between the T_g of the individual neat polymers, which, together with the PLOM observation indicated complete miscibility in the amorphous phase and no macroscopic phase separation. DSC and WAXS results indicated that a fraction of the PA6 chains cocrystallized within the PA410 unit cells when the fraction of PA6 was less than 50%. For the blends containing a majority fraction of PA6, separate crystallization of PA6 rich and PA410 rich phases was favored. The mechanical properties of the blends, such as Young's modulus, impact strength and strain at break changed with composition locating in between the neat polymers, which agrees with the typical character of compatible blends.

ACKNOWLEDGEMENTS

Supporting Information (SI)

The equilibrium melting point T_m^0 values(Table SI-1), optical micrographs of the samples (Figure SI-1), the calculation method of the intensity ratio from WAXS data (Figure SI-2), WAXS data (Figure SI-3), SAXS data (Figure SI-4), the long period values of the samples (Figure SI-5), L_p values at 210 ºC (Figure SI-6), the chemical structures of PA6, PA410 and PA6/PA410 blend (Figure SI-7) and the density values of PA6/PA410 blends (Figure SI-8).

REFERENCES

1.   Aeschelmann, F.; Carus, M., Biobased building blocks and polymers in the world: capacities, production, and applications–status quo and trends towards 2020. *Ind. Biotechnol.* **2015**, 11(3), 154-159, DOI: 10.1089/ind.2015.28999.fae.

2.   Ruehle, D. A.; Perbix, C.; Castaneda, M.; Dorgan, J. R.; Mittal, V.; Halley, P.; Martin, D., Blends of biorenewable polyamide-11 and polyamide-6,10. *Polymer* **2013,** *54* (26), 6961-6970, DOI: 10.1016/j.polymer.2013.10.013.

3.   Moran, C. S.; Barthelon, A.; Pearsall, A.; Mittal, V.; Dorgan, J. R., Biorenewable blends of polyamide-4,10 and polyamide-6,10. *J. Appl. Polym. Sci.* **2016,** *133* (45), 10.1002/app.43626.

4.   Wang, L.-l.; Dong, X.; Wang, X.-r.; Zhu, G.-y.; Li, H.-q.; Wang, D.-j., High performance long chain polyamide/calcium silicate whisker nanocomposites and the effective reinforcement mechanism. *Chin. J. Polym. Sci.* **2016,** *34* (8), 991-1000, DOI: 10.1007/s10118-016-1812-6.

5.   Wang, L.; Dong, X.; Huang, M.; Wang, D., Transient microstructure in long alkane segment polyamide: deformation mechanism and its temperature dependence. *Polymer* **2016,** *97*, 217-225, DOI: 10.1016/j.polymer.2016.05.038.

6.   Wang, L.; Dong, X.; Huang, M.; Müller, A. J.; Wang, D., The effect of microstructural evolution during deformation on the post-yielding behavior of self-associated polyamide blends. *Polymer* **2017,** *117*, 231-242, DOI: 10.1016/j.polymer.2017.04.038.

7.   Wang, L.; Dong, X.; Huang, M.; Müller, A. J.; Wang, D., Self-associated polyamide alloys with tailored polymorphism transition and lamellar thickening for advanced mechanical application. *ACS Appl. Mater.***2017,** *9* (22), 19238-19247, DOI: 10.1021/acsami.7b04691.

8.   Breuer, O.; Sundararaj, U., Big returns from small fibers: A review of polymer/carbon nanotube composites. *Polym. Compos.* **2004,** *25* (6), 630-645, DOI: 10.1002/pc.20058.

9.   Shin, Y. B.; Ha, H. M.; Han, H. D., Morphological, Rheological, and Mechanical Properties of Polyamide 6/Polypropylene Blends Compatibilized by Electron-Beam Irradiation in the Presence of a Reactive Agent. *Materials* **2016,** *9* (5), DOI: 10.3390/ma9050342.

10.   Fu, D.; Kuang, T.; Chen, F.; Lee, L. J.; Peng, X., Fabrication of high strength PA6/PP blends with pressure-induced-flow processing. *Mater. Chem. Phys.* **2015,** *164*, 1-5, DOI: 10.1016/j.matchemphys.2015.08.043.

11.   Heino, M.; Hietaoja, P.; Seppälä, J.; Harmia, T.; Friedrich, K., Studies on fracture behavior of tough PA6/PP blends. *J. Appl. Polym. Sci.* **1997,** *66* (12), 2209-2220, DOI: 10.1002/(SICI)1097-4628(19971219)66:12<2209::AID-APP2>3.0.CO;2-K.

12.   Cosas Fernandes, J. P.; Castro, L. D. C.; Mareau, V. H.; Pessan, L. A.; Gonon, L., New insights on the compatibilization of PA6/ABS blends: A co-localized AFM-Raman study. *Polymer* **2018,** *146*, 151-160, DOI: 10.1016/j.polymer.2018.05.012.

13.   Sui, X.; Xie, X.-M., Creating super-tough and strong PA6/ABS blends using multi-phase compatibilizers. *Chin. Chem. Lett.* **2019,** *30* (1), 149-152, DOI: 10.1016/j.cclet.2018.04.035.

14.   Castro, L. D. C.; Oliveira, A. D.; Kersch, M.; Altstädt, V.; Pessan, L. A., Effects of mixing protocol on morphology and properties of PA6/ABS blends compatibilized with MMA-MA. *J. Appl. Polym.* **2016,** *133* (27), DOI: 10.1002/app.43612.

15.   Agrawal, P.; Araujo, E. M.; Alves de Melo, T. J., Influence of reactive compatibilizers on the rheometrical and mechanical properties of PA6/LDPE and PA6/HDPE blends. *J. Mater. Sci.* **2010,** 45, 496–502, DOI: 10.1007/s10853-009-3967-9.

16.   Kudva, R.A., Keskkula, H. and Paul, D.R., Morphology and mechanical properties of compatibilized nylon 6/polyethylene blends. *Polymer* 1999, *40*(22), 6003-6021. DOI: 10.1016/S0032-3861(98)00829-5.

17.   Kim, B.K., Park, S.Y. and Park, S.J., Morphological, thermal and rheological properties of blends: Polyethylene/nylon-6, polyethylene/nylon-6/(maleic anhydride-g-polyethylene) and (maleic anhydride-g-polyethylene)/nylon-6. *Eur. Polym. J.* **1991**, 27(4-5), 349-354, DOI: 10.1016/0014-3057(91)90186-R.

18.   Wang, X. C.; Zheng, Q.; Yang, G. S., Influence of preparation methods on structure and properties of PA6/PA66 blends: A comparison of melt-mixing and in situ blending. *J. Polym. Sci.B: Polymer Physics* **2007,** *45* (10), 1176-1186, DOI: 10.1002/polb.21103.

19.   Lin, X.; Qian, Q.; Xiao, L.; Chen, Q.; Huang, Q.; Zhang, H., Influence of Reactive Compatibilizer on the Morphology, Rheological, and Mechanical Properties of Recycled Poly(Ethylene Terephthalate)/Polyamide 6 Blends. *J. Macromol. Sci. B* **2014,** *53* (9), 1543-1552, DOI: 10.1080/00222348.2014.946840.

20.   Wang, L.; Dong, X.; Gao, Y.; Huang, M.; Han, C. C.; Zhu, S.; Wang, D., Transamidation determination and mechanism of long chain-based aliphatic polyamide alloys with excellent interface miscibility. *Polymer* **2015,** *59,* 16-25, DOI: 10.1016/j.polymer.2014.12.058.

21.   Hemlata; Maiti, S. N., Nonisothermal crystallization kinetics of PA6 and PA6/SEBS-g-MA blends. *J. Polym. Res.* **2012,** *19* (8), 9926, DOI: 10.1007/s10965-012-9926-1.

22.   Gomes, A. C. O.; Soares, B. G.; Oliveira, M. G.; Pessan, L. A.; Paranhos, C. M., Influence of compatibilizer content on PA/NBR blends properties: Unusual characterization and evaluation methods. *J. Appl. Polym.* **2013,** *127* (3), 2192-2200, DOI: 10.1002/app.37792.

23.   Cote, P.; Brisson, J., Miscibility of Polyamide Blends. 2. Thermal Study of Poly(hexamethylene isophthalamide)/Nylon-n,m Blends. *Macromolecules* **1994,** *27* (25), 7329-7338, DOI: 10.1021/ma00103a014.

24.   Ellis, T. S., Miscibility in blends of aliphatic polyamides and an aromatic polyamide, nylon 3Me6T. *Polymer* **1988,** *29* (11), 2015-2026, DOI: 10.1016/0032-3861(88)90175-9.

25.   Ellis, T. S., Miscibility and immiscibility of polyamide blends. *Macromolecules* **1989,** *22* (2), 742-754, DOI: 10.1021/ma00192a039.

26.   Ellis, T. S., Critical miscibility limits in blends of aliphatic polyamides containing an aromatic polyamide. *Polymer* **1990,** *31* (6), 1058-1064, DOI: 10.1016/0032-3861(90)90253-U.

27.   Ellis, T. S., Influence of structure on phase behavior of polyamide blends. *Macromolecules* **1991,** *24* (13), 3845-3852, DOI: 10.1021/ma00013a017.

28.   Ellis, T. S., Estimating interactions in blends of polyamides, polyesters and polycarbonate using copolymers. *Macromol. Symp.* **1996,** *112* (1), 47-54, DOI: 10.1002/masy.19961120108.

29.   Ellis, T. S., Miscibility of polyamide blends: effects of configuration. *Polymer* **1995,** *36* (20), 3919-3926, DOI: 10.1016/0032-3861(95)99786-T.

30.   Zhang, G. Z.; Yoshida, H.; Kawai, T., Miscibility of Nylon 66 and Nylon 48 blend evaluated by crystallization dynamics. *Thermochim. Acta* **2004,** *416* (1-2), 79-85, 10.1016/j.tca.2003.01.002.

31.   Verma, A.; Deopura, B. L.; Sengupta, A. K., A study on blends of nylon-6 and nylon-66. *J. Appl. Polym* **1986,** *31* (3), 747-762, DOI: 10.1002/app.1986.070310301.

32.   Wei, M.; Shin, I. D.; Urban, B.; Tonelli, A. E., Partial miscibility in a nylon-6/nylon-66 blend coalesced from their common α-cyclodextrin inclusion complex. *J. Polym. Sci. B Polym. Phys.* **2004,** *42* (8), 1369-1378, DOI: 10.1002/polb.20018.

33.   Yu, L.; Dean, K.; Li, L., Polymer blends and composites from renewable resources. *Prog. Polym. Sci.* **2006,** *31* (6), 576-602, DOI: 10.1016/j.progpolymsci.2006.03.002.

34.   Sionkowska, A., Current research on the blends of natural and synthetic polymers as new biomaterials: Review. *Prog. Polym. Sci.* **2011,** *36* (9), 1254-1276, DOI: 10.1016/j.progpolymsci.2011.05.003.

35.   Feldman, D., Polyblend Compatibilization. *J. Macromol. Sci. A.* **2005,** *42* (5), 587-605, DOI: 10.1081/MA-200056331.

36.   Madhavan Nampoothiri, K.; Nair, N. R.; John, R. P., An overview of the recent developments in polylactide (PLA) research. *Bioresour. Technol.* **2010,** *101* (22), 8493-8501, DOI: 10.1016/j.biortech.2010.05.092.

37.   Nitz, H.; Semke, H.; Mülhaupt, R., Influence of Lignin Type on the Mechanical Properties of Lignin Based Compounds. *Macromol. Mater. Eng.* **2001,** *286* (12), 737-743, DOI: 10.1002/1439-2054(20011201)286:12<737::AID-MAME737>3.0.CO;2-2.

38.   Amass, W.; Amass, A.; Tighe, B., A review of biodegradable polymers: uses, current developments in the synthesis and characterization of biodegradable polyesters, blends of biodegradable polymers and recent advances in biodegradation studies. *Polym. Int.* **1998,** *47* (2), 89-144, DOI: 10.1002/(SICI)1097-0126(1998100)47:2<89::AID-PI86>3.0.CO;2-F.

39.   Auras, R.; Harte, B.; Selke, S., An Overview of Polylactides as Packaging Materials. *Macromol. Biosci.* **2004,** *4* (9), 835-864, DOI: 10.1002/mabi.200400043.

40.   Chandra, R.; Rustgi, R., Biodegradable polymers. *Prog. Polym. Sci.* **1998,** *23* (7), 1273-1335, DOI: 10.1016/S0079-6700(97)00039-7.

41.   Gross, R. A.; Kalra, B., Biodegradable Polymers for the Environment. *Science* **2002,** *297* (5582), 803, DOI: 10.1126/science.297.5582.803.

42.   Ikada, Y.; Tsuji, H., Biodegradable polyesters for medical and ecological applications. *Macromol. Rapid Commun.* **2000,** *21* (3), 117-132, DOI: 10.1002/(SICI)1521-3927(20000201)21:3<117::AID-MARC117>3.0.CO;2-X.

43.   Marra, K. G.; Szem, J. W.; Kumta, P. N.; DiMilla, P. A.; Weiss, L. E., In vitro analysis of biodegradable polymer blend/hydroxyapatite composites for bone tissue engineering. *J. Biomed. Mater. Res.* **1999,** *47* (3), 324-335, DOI: 10.1002/(SICI)1097-4636(19991205)47:3<324::AID-JBM6>3.0.CO;2-Y.

44.   Martin, O.; Avérous, L., Poly(lactic acid): plasticization and properties of biodegradable multiphase systems. *Polymer* **2001,** *42* (14), 6209-6219, DOI: 10.1016/S0032-3861(01)00086-6.

45.   Azizi Samir, M. A. S.; Alloin, F.; Dufresne, A., Review of Recent Research into Cellulosic Whiskers, Their Properties and Their Application in Nanocomposite Field. *Biomacromolecules* **2005,** *6* (2), 612-626, DOI: 10.1021/bm0493685.

46.   Sudesh, K.; Abe, H.; Doi, Y., Synthesis, structure and properties of polyhydroxyalkanoates: biological polyesters. *Prog. Polym. Sci.* **2000,** *25* (10), 1503-1555, DOI: 10.1016/S0079-6700(00)00035-6.

47.   Koulouri, E. G.; Scourlis, E. C.; Kallitsis, J. K., Characterization of melt-mixed blends of poly(ether–ester) with various polyamides. *Polymer* **1999,** *40* (17), 4887-4896, DOI: 10.1016/S0032-3861(98)00707-1.

48.   Adhikari, R.; Michler, G. H., Influence of molecular architecture on morphology and micromechanical behavior of styrene/butadiene block copolymer systems. *Prog. Polym. Sci.* **2004,** *29* (9), 949-986, DOI: 10.1016/j.progpolymsci.2004.06.002.

49.   Kuo, S. W., Effect of copolymer compositions on the miscibility behavior and specific interactions of poly(styrene-co-vinyl phenol)/poly(vinyl phenyl ketone) blends. *Polymer* **2008,** *49* (20), 4420-4426, DOI: 10.1016/j.polymer.2008.08.002.

50.   Paul, D. R.; Barlow, J. W., A binary interaction model for miscibility of copolymers in blends. *Polymer* **1984,** *25* (4), 487-494, DOI: 10.1016/0032-3861(84)90207-6.

51.   Nakai, A.; Shiwaku, T.; Wang, W.; Hasegawa, H.; Hashimoto, T., Process and Mechanism of Phase Separation in Polymer Mixtures with a Thermotropic Liquid

Crystalline Copolyester as One Component. *Macromolecules* **1996,** *29* (18), 5990-6001, DOI: 10.1021/ma9512768.

52.   Puskas, J. E.; Kwon, Y.; Altstädt, V.; Kontopoulou, M., Blends of poly(2,6-dimethyl-1,4-phenylene oxide) (PPO) with polystyrene-based thermoplastic rubbers: A comparative study. *Polymer* **2007,** *48* (2), 590-597, DOI: 10.1016/j.polymer.2006.11.045.

53.   Karode, S. K.; Kulkarni, S. S.; Suresh, A. K.; Mashelkar, R. A., Molecular weight distribution in interfacial polymerization—model development and verification. *Chem. Eng. Sci.* **1997,** *52* (19), 3243-3255, DOI: 10.1016/S0009-2509(97)00138-3.

54.   Karode, S. K.; Kulkarni, S. S.; Suresh, A. K.; Mashelkar, R. A., New insights into kinetics and thermodynamics of interfacial polymerization. *Chem. Eng. Sci.* **1998,** *53* (15), 2649-2663, DOI: 10.1016/S0009-2509(98)00083-9.

55.   Ellis, T. S., Mixing relationships in aliphatic polyamide blends. *Polymer* **1992,** *33* (7), 1469-76, DOI: 10.1016/0032-3861(92)90124-F.

56.   Otaegi, I.; Aramburu, N.; Muller, A. J.; Guerrica-Echevarria, G., Novel Biobased Polyamide 410/Polyamide 6/CNT Nanocomposites. *Polymers (Basel)* **2018,** *10* (9), DOI: 10.3390/polym10090986.

57.   Liu, J.; Jungnickel, B. J., Crystallization kinetical and morphological peculiarities in binary crystalline/crystalline polymer blends. *J. Polym. Sci. B Polym. Phys.* **2007,** *45* (15), 1917-1931, DOI: 10.1002/polb.21162.

58.   Mandelkern, L., *Crystallization of Polymers: Volume 2, Kinetics and Mechanisms*. Cambridge University Press, Cambridge, 2004.

59.   Holmes, D.; Bunn, C.; Smith, D., The crystal structure of polycaproamide: Nylon 6. *J. Polym. Sci.* **1955,** *17* (84), 159-177, DOI: 10.1002/pol.1955.120178401.

60.   Xanthos, M.; Parmer, J. F.; La Forest, M. L.; Smith, G. R., Impact modification of aromatic/aliphatic polyamide blends: Effects of composition and processing conditions. *J. Appl. Polym. Sci.* **1996,** *62* (8), 1167-1177, DOI: 10.1002/(SICI)1097-4628(19961121)62:8<1167::AID-APP5>3.0.CO;2-G.

61.   Persyn, O.; Miri, V.; Lefebvre, J. M.; Ferreiro, V.; Brink, T.; Stroeks, A., Mechanical behavior of films of miscible polyamide 6/polyamide 6I-6T blends. *J. Polym. Sci. B Polym. Phys.* **2006,** *44* (12), 1690-1701, DOI: 10.1002/polb.20825.

62.   Persyn, O.; Miri, V.; Lefebvre, J. M.; Depecker, C.; Gors, C.; Stroeks, A., Structural organization and drawability in polyamide blends. *Polym. Eng. Sci.* **2004,** *44* (2), 261-271, DOI: 10.1002/pen.20025.

63.   Jones, N.; Atkins, E.; Hill, M.; Cooper, S.; Franco, L., Chain-folded lamellar crystals of aliphatic polyamides. Investigation of nylons 4 8, 4 10, 4 12, 6 10, 6 12, 6 18 and 8 12. *Polymer* 1997, 38 (11), 2689-2699, DOI: 10.1016/S0032-3861(97)85603-0 .

64.   Eguiaźbal, J. I.; Ferńndez-Berridi, M. J.; Iruin, J. J.; Maiza, I., PBT/PAr mixtures: Influence of interchange reaction on mechanical and thermal properties. *J. Appl. Polym* **1996,** *59* (2), 329-337, DOI: 10.1002/(SICI)1097-4628(19960110)59:2<329::AID-APP17>3.0.CO;2-R.

65.   Martínez, J. M.; Eguiazábal, J. I.; Nazábal, J., Poly(butylene terephthalate)/phenoxy blends: Synergistic behavior in mechanical properties. *J. Macromol. Sci. B* **1991,** *30* (4), 345-355, 10.1080/00222349108219482.

66.   Kim, J. H.; Min, B. R.; Kang, Y. S., Thermodynamic Model of the Glass Transition Behavior for Miscible Polymer Blends. *Macromolecules* **2006,** *39* (3), 1297-1299, DOI: 10.1021/ma052436a.

67.   Ellis, T. S., Mixing relationships in aliphatic polyamide blends. *Polymer 1992*, 33(7), 1469-1476, DOI: 10.1016/0032-3861(92)90124-F.

68.   Ramiro, J.; Eguiazábal, J. I.; Nazábal, J., Synergistic mechanical behaviour and improved processability of poly(ether imide) by blending with poly(trimethylene terephthalate). *Polym. Adv. Technol.* **2003,** *14* (2), 129-136, DOI: 10.1002/pat.340.

69.   Rodríguez, J. L.; Eguiazábal, J. I.; Nazábal, J., Physical properties of poly(butylene terephthalate)/poly(ester-carbonate) blends. *J. Macromol. Sci. B***1997,** *36* (6), 773-787, DOI: 10.1080/00222349708212401.

70.   Vallejo, F. J.; Eguiazábal, J. I.; Nazábal, J., Solid state features and mechanical properties of PEI/PBT blends. *J. Appl. Polym. Sci.***2001,** *80* (6), 885-892, DOI: 10.1002/1097-4628(20010509)80:6<885::AID-APP1166>3.0.CO;2-D.

71.   Martinez, J. M.; Eguiaabal, J. I.; Nazabal, J., Miscibility level and properties of poly(ether imide)/poly(ethylene terephthalate) blends. *J. Appl. Polym. Sci.* **1996,** *62* (2), 385-391, DOI: 10.1002/(SICI)1097-4628(19961010)62:2<385::AID-APP13>3.0.CO;2-0.

72.   Barlow, J. W.; Paul, D. R., Polymer blends and alloys - a review of selected considerations. *Polym. Eng. Sci.* **1981,** *21* (15), 985-96, DOI: 10.1002/pen.760211502.

73.   Joseph, E. A.; Lorenz, M. D.; Barlow, J. W.; Paul, D. R., Mechanical properties of miscible polycarbonate-copolyester blends. *Polymer* **1982,** *23* (1), 112-22, DOI: 10.1016/0032-3861(82)90024-6.

74.   Kleiner, L. W.; Karasz, F. E.; Macknight, W. J., Compatible glassy polyblends based upon poly(2,6-dimethyl-1,4-phenylene oxide): tensile modulus studies. *Polym. Eng. Sci.* **1979,** *19* (7), 519-24, DOI: 10.1002/pen.760190710.

75.   Arzak, A.; Eguiazábal, J. I.; Nazábal, J., Mechanical performance of directly injection-molded PEEK/PEI blends at room and high temperature. *J. Macromol. Sci. Phys. B* **1997,** *36* (2), 233-246, DOI: 10.1080/00222349708220428.

76.   Ramiro, J.; Eguiazábal, J. I.; Nazábal, J., New Miscible Poly(ether imide)/Poly(phenyl sulfone) Blends. *Macromol. Mater. Eng.* **2006,** *291* (6), 707-713, DOI: 10.1002/mame.200500429.

77.   Prinos, J.; Tselios, C.; Bikiaris, D.; Panayiotou, C., Properties of miscible blends of polyglutarimide with poly(styrene-co-maleic anhydride). *Polymer* **1997,** *38* (24), 5921-5930, DOI: 10.1016/S0032-3861(97)00167-5.

78.   Aranburu, N.; Eguiazabal, J. I., Compatible blends of polypropylene with an amorphous polyamide. *J. Appl. Polym. Sci.* **2013,** *127* (6), 5007-5013, DOI: 10.1002/app.38090.

79.   Gonzalez, I.; Eguiazabal, J. I.; Nazabal, J., Toughening and brittle-tough transition in blends of an amorphous polyamide with a modified styrene/ethylene-butylene/styrene triblock copolymer. *Polym. Eng. Sci.* **2009,** *49* (7), 1350-1356, DOI: 10.1002/pen.21250.

80.   Wang, Y.; Wang, W.; Peng, F.; Liu, M.; Zhao, Q.; Fu, P.-F., Morphology of Nylon 1212 toughened with a maleated EPDM rubber. *Polym. Int.* **2009,** *58* (2), 190-197, DOI: 10.1002/pi.2514.